THE ASTROPHYSICAL JOURNAL, 491:216–232, 1997 December 10

HYDRODYNAMICS OF CLOUD COLLISIONS IN TWO DIMENSIONS: THE FATE OF CLOUDS IN A MULTIPHASE MEDIUM

FRANCESCO MINIATI,[1,2] T. W. JONES,[1] ANDREA FERRARA,[3] AND DONGSU RYU[4,5]

Received 1997 June 13; accepted 1997 July 24

ABSTRACT

We have studied head-on collisions between equal-mass, mildly supersonic H I clouds (Mach number 1.5 with respect to the background medium) through high-resolution numerical simulations in two dimensions. We explore the role of various factors, including the radiative cooling parameter, $\eta = \tau_{\rm rad}/\tau_{\rm coll}$ ($\tau_{\rm coll} = R_c/v_c$), evolutionary modifications on the cloud structure, and the symmetry of the problem. Self-gravity is not included. Radiative losses are taken into account explicitly and not approximated with an isothermal adiabatic index $\gamma \approx 1$, which, in fact, leads to very different results. We assume a standard two-phase interstellar medium (ISM) model where clouds are characterized by a temperature $T_c = 74$ K and number density $n_c = 22$ cm^{-3} and are in pressure equilibrium with the surrounding warm intercloud medium (WIM), with a density contrast $\chi = \rho_c/\rho_i = 100$. In particular, we study collisions for the adiabatic ($\eta \gg 1$) and radiative ($\eta = 0.38$) cases that may correspond to small ($R_c \leq 0.4$ pc for an assumed WIM) or large ($R_c \sim 1.5$ pc) clouds, respectively. In addition to a standard case of identical "nonevolved" clouds, we also consider the collision of identical clouds, "evolved" through independent motion within the intercloud gas, over one crushing time before collision. This turns out to be about the mean collision time for such clouds in the ISM. The presence of bow shocks and ram pressure from material in the cloud wake alters these interactions significantly with respect to the standard case. In some cases, we removed the mirror symmetry from the problem by colliding initially identical clouds "evolved" to different ages before impact. In those cases, the colliding clouds have different density and velocity structures, so that they provide a first insight on the behavior of more complex interactions.

In our adiabatic collisions, the clouds are generally disrupted and convert their gas into the warm phase of the ISM. Although the details depend on the initial conditions, the two colliding clouds are converted into a few low-density contrast ($\chi \sim 5$) clumps at the end of the simulations.

By contrast, for *symmetric* radiative cases, we find that the two clouds coalesce, and there are good chances for a new massive cloud to be formed. Almost all the initial kinetic energy of the two clouds is radiated away during such collisions. On the other hand, for both adiabatic and radiative collisions, symmetry breaking leads to major differences. Most importantly, asymmetric collisions have a much greater tendency to disrupt the two clouds. Portions of individual clouds may be sheared away, and instabilities along the interfaces between the clouds and with the intercloud medium are enhanced. In addition, radiative cooling is less efficient in our asymmetric interactions, so that those parts of the clouds that initially seem to merge are more likely to reexpand and fade into the warm intercloud medium. Since the majority of real cloud collisions should be asymmetric for one reason or another, we conclude that most gasdynamical diffuse cloud collisions will be disruptive, at least in the absence of significant self-gravity or a significant magnetic field.

Subject headings: hydrodynamics — ISM: clouds — ISM: kinematics and dynamics

1. INTRODUCTION

Interstellar cloud collisions (hereafter CCs) are important for the dynamical evolution of galaxies. Indeed, CCs turn out to be relevant in a large variety of important processes occurring in the interstellar medium (ISM), such as star formation, dissipation of kinetic energy, and gas-phase transitions. In addition, they affect the gaseous structure and the energy budget of galaxies, along with the mass spectrum of diffuse ISM clouds and their evolution.

CCs were first studied by Stone (1970a, 1970b), who was concerned mainly with the evolution of interstellar clouds, and especially of their structure. In his pioneering papers, he found that, despite the very high compression experienced by clouds during CCs, star formation is not enhanced. Instead, he found that colliding clouds lose mass and that large-scale perturbations and internal motions (approximately radial) form within the clouds, which do not decay before the next collision. Thus, cloud hydrostatic equilibrium is severely compromised, suggesting the idea of clouds with smooth density distribution profiles instead of (clouds as) sharply bounded objects (Stone 1970b). Smith (1980) performed one-dimensional numerical simulations and concluded that, in a dusty ISM, low Mach number (≤ 5) collisions are the most likely to trigger star formation. Further investigations have been carried out by Gilden (1984) and Lattanzio et al. (1985, hereafter LMPS) using two- and three-dimensional models, respectively. These authors studied the role of various parameters involved in

[1] School of Physics and Astronomy, 116 Church Street, SE, University of Minnesota, Minneapolis, MN 55455; min@msi.umn.edu, twj@astro.spa.umn.edu.

[2] Dipartimento di Astronomia, Università di Firenze, I-50125 Firenze, Italy.

[3] Osservatorio Astrofisico Arcetri, Largo Enrico Fermi 5, I-50125 Firenze, Italy; ferrara@arcetri.astro.it.

[4] Department of Astronomy and Space Science, Chungnam National University, Daejeon, 305-764, Korea; ryu@sirius.chungnam.ac.kr.

[5] Department of Astronomy, University of Washington, Box 351580, Seattle, WA 98195-1580.

the collisions, such as the relative size of the clouds, their masses, and their impact parameter. They generally concluded that CCs more often lead to disruption than to coalescence or gravitational collapse of the clouds. This again has been interpreted as evidence that the ISM should be described as a continuous distribution of gas streams and turbulent eddies (LMPS; Hunter et al. 1986), which contrasts with most dynamical models for the ISM that depict it more simply as pressure-confined neutral cold clouds moving through a warm intercloud medium (WIM) (see e.g., Norman & Ferrara 1996, Vazquez-Semadeni, Passot, & Pouquet 1995, and references therein). This point is so important that further investigation of the final fate of the clouds is worthwhile. In fact, it turns out that CCs are very frequent, with a rate of about once every 10^6–10^7 yr for individual clouds, leading to a total of approximately one cloud collision every 100 yr in the Galaxy (Stone 1970a, 1970b; Spitzer 1978; Hausman 1981). Their outcome could profoundly affect the mass interchange of the various phases that are believed to exist in the ISM.

CCs may also be responsible for the buildup of the observed mass spectrum of diffuse clouds (Dickey & Garwood 1989; Solomon & Rivolo 1989; Oort 1954; Field & Saslaw 1965; Field & Hutchings 1968; Penston et al. 1969; Cowie 1980; Hausman 1982; Pumphrey & Scalo 1983; Struck-Marcell & Scalo 1984; Fleck 1996; Mousumi & Chanda 1996). Early models suggested a hierarchical scenario in which small clouds, formed in H II regions out of much larger clouds through star formation, are supposed to undergo repeated inelastic collisions and coalescence, thus engendering new clouds of larger mass (Oort 1954; Field & Saslaw 1965). Yet an accurate model should take into account the detailed outcome of CC processes. In their model, Field & Saslaw (1965) assume, for example, that each CC leads to coalescence, an uncertain assumption as discussed above and by several authors including Stone (1970a, 1970b), Hausman (1981), Gilden (1984), and Klein, McKee, & Wood (1995, hereafter KMW).

In addition, CCs are relevant for the energy budget and gaseous structure of a galaxy. Clouds are accelerated in H II regions (Field & Saslaw 1965) and by supernovae. The turbulence pressure associated with their motion determines the vertical structure of the cold neutral phase in the ISM (McKee 1990; Ferrara 1993; Norman & Ferrara 1996). The bulk motions, on the other hand, are dissipated through inelastic collisions (Spitzer 1978). It is also worthwhile to mention that the amount of energy dissipated during CCs depends on the dust content and on the metallicity of the ISM, as discussed by Ricotti, Ferrara, & Miniati (1997, hereafter RFM), who determined the dependence of the elasticity of a collision on parameters such as relative cloud velocity, size, metallicity, and dust-to-gas ratio. Their paper gives a useful overview of the characteristics of collisions and represents a complementary study to the present one.

The present paper is devoted to a further investigation of the consequences of CCs. In particular, we hope to determine the fate (i.e., survival, dispersal in the WIM, coalescence, or fragmentation) of clouds in a two-phase ISM with canonical properties. In addition, we investigate the evolution of the cloud kinetic energy. This could be retained by the clouds as thermal energy, radiated away during the collision, or transferred to the WIM. Very recently, some attention has been devoted to the hydrodynamical details that characterize the flow structure in CCs (KMW; Kimura & Tosa 1996). KMW have pointed out important instabilities that develop in the collision process. In particular, they have shown that small-amplitude surface perturbations may lead to the development of the "bending mode instability" (Vishniac 1994) in the cloud shocks, which, in turn, causes the colliding material to form filamentary structures. Our work extends the KMW study by adding individual cloud evolution through the intercloud medium, before the collision. This increases the realism of the simulations by taking into account the role of cloud bow shocks and wakes and of nonuniform cloud structures. By colliding two clouds that have undergone different amounts of prior evolution, we introduce a simple means to relax the symmetry imposed in most previous calculations. This turns out to alter dramatically the result of the interactions in ways that extend beyond the direct influence of the bending mode. We still limit for now our attention to head-on two-dimensional gasdynamical collisions between clouds of (initially) equal mass and Mach number.

The plan of this paper is as follows. In § 2, we describe the physical problem under investigation and discuss the assumptions made. In § 3, we describe the computational setup. In § 4, we present the main results of this study. A discussion is given in § 5, whereas the summary and conclusions are in § 6.

2. DESCRIPTION OF THE PROBLEM

It is known (e.g., Stone 1970a, 1970b; KMW) that collisions between identical homogeneous clouds are generally characterized by three main evolutionary stages, as shown in Figure 1. These are (1) a *compression phase* in which a shock wave forms in each cloud and propagates through it, converting cloud kinetic energy into thermal energy. If radiative cooling is efficient, a fair fraction of this thermal energy is radiated away. Otherwise, the pressure becomes high enough to drive shocks outward from the center of the collision. At the end of the compression phase, the gas is highly compressed into a thin (compared with the initial cloud size) layer, whose thickness depends on the amount of radiative losses (Fig. 1*a* [*top panel*] and the top panel of Fig. 2). (2) A *reexpansion phase* begins when shocks generated during the collision emerge into the intercloud medium. During this phase, a rarefaction wave propagates backward into the clouds, forming a central low-pressure and low-density region (Fig. 1*a* [*bottom panel*] and Fig. 2). Also, a fast sheet of ejecta emerges from the contact discontinuity between the merged clouds. This structure, which appears like a "jet" in two-dimensional collisions with mirror symmetry between the clouds, is subject to Kelvin-Helmholtz instabilities (KHIs) (Fig. 3, *middle panel*). Also, during the reexpansion phase, a reverse shock forms and interacts with the expanding cloud material. As will be shown in § 4, the qualitative and quantitative details of this phase depend strongly on the adiabaticity and symmetry of the collision. (3) There follows a *collapse phase* when the expansion is halted by the external surrounding medium. The pressure inside the clouds is by now much lower than in the external ambient medium, so that the cloud material is driven back toward the merged cloud core. As pointed out in the literature, during this phase Rayleigh-Taylor instabilities (RTIs) become very important, especially in disrupting the cloud surface and ablating material away from it (Fig. 1*b*, *top panel*). The details of the evolution of these properties are

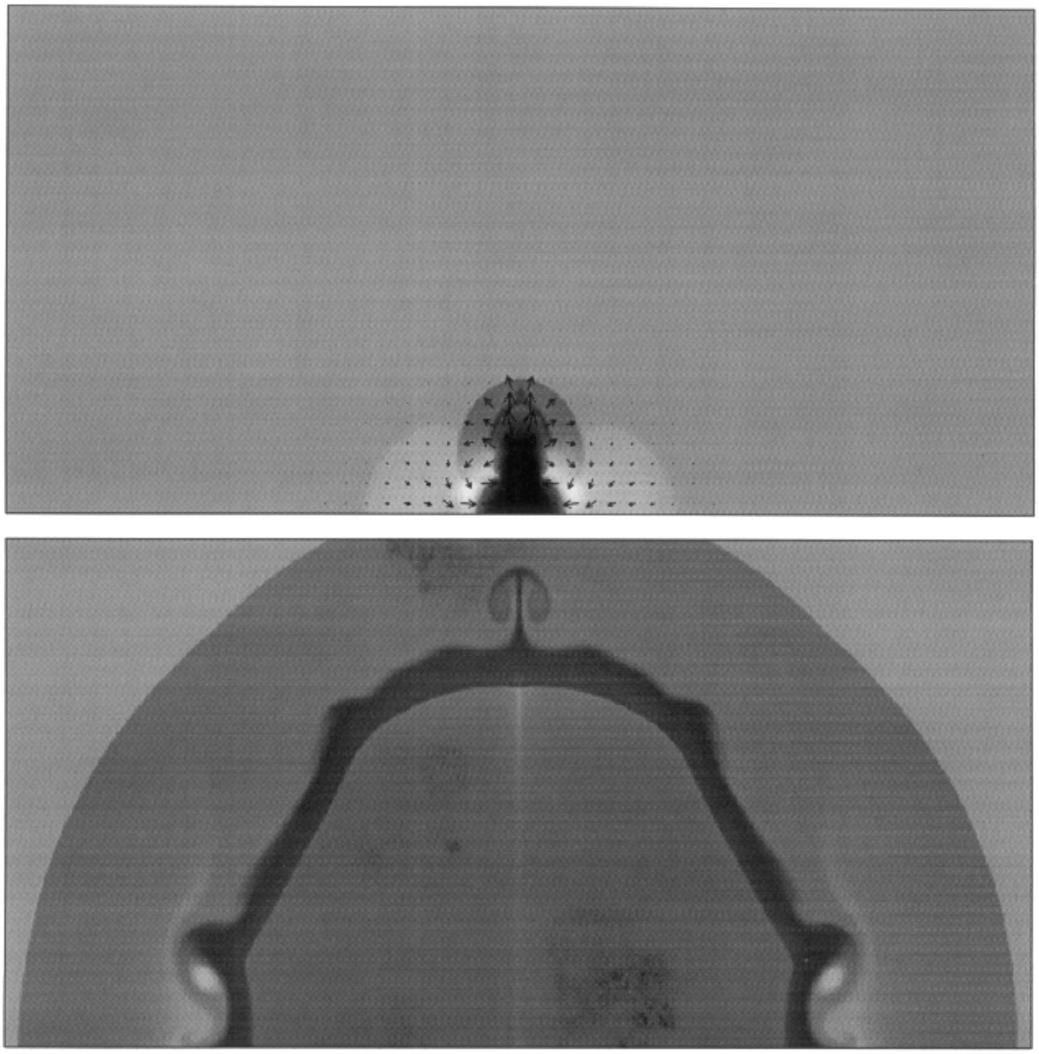

FIG. 1*a*

FIG. 1.—Inverted gray-scale images of tanh (log ρ) for case 1. The vector display of the velocity field is superimposed. (1*a*, *top*) The compression phase at $t = 1.5\tau_{\rm coll}$ with outflow at the side of the contact discontinuity. (1*a*, *bottom*) The reexpansion phase at $8.2\tau_{\rm coll}$, with the formation of a dense shell-like structure. The top and bottom panels of 1*b*, correspond, respectively, to the collapse phase at $t = 37.5\tau_{\rm coll}$ and to the dispersal phase at $t = 67.5\tau_{\rm coll}$. The dramatic development of KHIs and RTIs is evident.

obviously closely related to the previous reexpansion phase and thus depend as well on the adiabaticity of the collision. Under some circumstances, it appears that one should add (4) a *dispersal phase*, since the original clouds may be largely converted to the WIM (Fig. 1*b*, *bottom panel*).

In the absence of self-gravity, and for a Mach number high enough that Mach scaling applies (KMW), the primary parameter controlling head-on collisions between identical clouds is

$$\eta = \frac{N_{\rm rad}}{n_c R_c}, \tag{1}$$

where $N_{\rm rad}$ is the radiative cooling column density, while n_c and R_c are the cloud number density and radius, respectively. Note that this definition for η agrees with the one in equation (5) of RFM; their adjustable parameter α is here taken to be equal to unity. Thus, when comparing the two sets of results, our η should be divided by $\alpha^{-1} \sim 3$. If we express $N_{\rm rad}$ in terms of the radiative cooling time $\tau_{\rm rad}$, n_c, and the individual cloud velocity v_c ($N_{\rm rad} = n_c v_c \tau_{\rm rad}$),

$$\eta = \frac{\tau_{\rm rad}}{R_c/v_c} = \frac{\tau_{\rm rad}}{\tau_{\rm coll}}, \tag{2}$$

where, according to Spitzer (1978),

$$\tau_{\rm rad} = \frac{3}{2}\frac{kT}{n\Lambda(n, T, Z)}, \tag{3}$$

and $\Lambda(n, T, Z)$ is the interstellar cooling function depending on number density n, temperature T, and metallicity Z. We have introduced the collision time $\tau_{\rm coll} = R_c/v_c$, which is a natural timescale for CCs and is about the time over which the compression phase occurs. The collision is adiabatic if $\eta \gg 1$, radiative if $\eta \sim 1$, and isothermal if $\eta \ll 1$. Since, according to equation (3), $\tau_{\rm rad}$ only depends on the density and temperature of the cloud (and on the metallicity, Z), then, from equation (2), $\eta \propto v_c/R_c$, and we can infer that small supersonic clouds undergo primarily adiabatic collisions, whereas interactions between large, slow clouds are mostly radiative or isothermal. Since in the adiabatic case

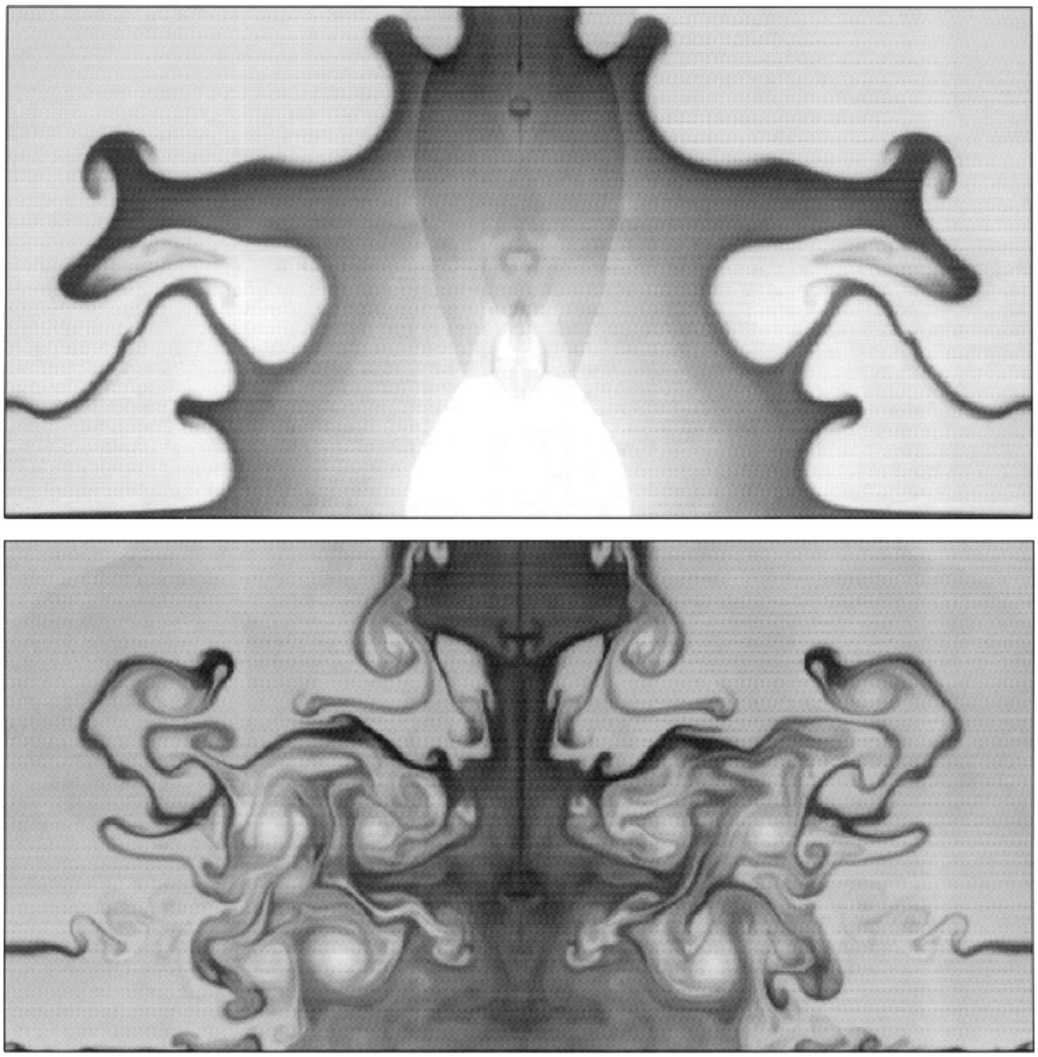

FIG. 1*b*

$\tau_{\rm coll} \ll \tau_{\rm rad}$, there is not enough time for the thermal energy to be radiated away during the collision. On the other hand, in the radiative regime $\tau_{\rm rad} \sim \tau_{\rm coll}$, and during the collision a significant fraction of the energy associated with the clouds is converted into radiation. This fraction is even larger in the isothermal case.

Occasionally in calculations such as the present ones, strong radiative cooling is taken into account approximately by setting the gas adiabatic index $\gamma \sim 1$. That is, the flow is assumed to be inherently isothermal. This method allows much greater compression in the flow than the usual $\gamma = 5/3$ case, an effect similar to that expected during a radiative compression. However, this approach *is not appropriate* for the problem at hand. As long as total energy is conserved, even a $\gamma \sim 1$ gas will have a substantially higher pressure behind a strong shock rather than in front of it. That leads in the present situation to strong pressure gradients that drive gas flows out of the impact region during a collision. On the other hand, when radiative cooling is included properly, the thermal energy is removed from the interaction region (during the collision) before the reexpansion takes place, significantly reducing forces that drive gas away from that region. We carried out comparison simulations using $\gamma \sim 1$ to approximate strong radiative cooling. They had properties very different from the properly radiatively cooled flows, actually resembling more closely the adiabatic flows for the reasons already mentioned.

Considering weakly radiative or fully adiabatic cases, on the other hand, it is worthwhile to notice that we performed several tests with $1.5 \leq \eta \leq \infty$ and did not find any substantial differences among them in either qualitative or quantitative terms. This means that even though our adiabatic simulations are characterized by $\eta \gg 1$, they also represent cases with $\eta \geq 1.5$ reasonably well.

In this paper, we restrict our study to head-on collision of neutral hydrogen (H I) clouds and only consider supersonic clouds. In fact, according to Spitzer (1978), supersonic clouds should be the most common case for the ISM. We neglect for now the magnetic field. KMW and RFM included, in their calculations, a magnetic pressure term corresponding to an initially weak ($B \sim 1$ μG) magnetic field in order to limit the extraordinary compression otherwise occurring during radiative or isothermal collisions. However, a full MHD simulation was lacking. In complex flows, shear is typically more important to magnetic field behavior than compression (e.g., Frank et al. 1996; Jones, Ryu, & Tregillis 1996), and so full MHD may be expected to behave differently. We ignore any thermal conduction effects as well as self-gravity in the present simulations.

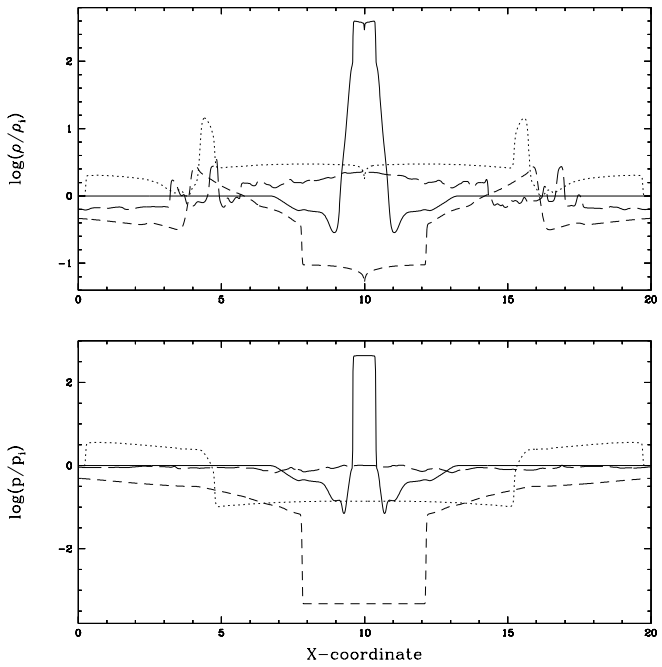

FIG. 2.—A cut through the grid along the X-axis ($Y = 0.3R_c$) for case 1. The top and bottom panels show a log plot of density and pressure, respectively. The solid lines refer to $t = 1.5\tau_{\rm coll}$, the dotted lines to $t = 8.2\tau_{\rm coll}$, the short-dashed lines to $t = 37.5\tau_{\rm coll}$, and the long-dashed lines to $t = 67.5\tau_{\rm coll}$.

We chose three different conditions for the clouds at impact, and for each investigated adiabatic and radiative flows, giving a total set of six cases. The simplest initial condition involves uniform, pressure-bound clouds, immediately adjacent and placed in motion at the start of the simulation in an initially uniform background. Thus, these collisions take place before the clouds have formed any structure because of their motions, i.e., they are "nonevolved." Although this case is not very realistic, it most closely resembles previous work (e.g., Stone 1970a, 1970b; LMPS; KMW), and since it produces clean demonstrations of the four stages of CCs, it is very useful as a "standard model." Next, to add some realism and to include nonuniform structures in a natural way, we also considered collisions between clouds that had evolved independently before impact. Those clouds were otherwise identical to the ones used in the "standard," "nonevolved" collisions. We considered two varieties of such "evolved" clouds. First, we followed collisions between two clouds after each had undergone an identical evolution time (being a so-called "crushing time," defined in eq. [4]), so that the impacting clouds still had a mirror symmetry. We alternatively allowed collisions between two clouds of somewhat different evolutionary ages. Since, during their evolution, the clouds become increasingly irregular because of KHIs and RTIs, these last collisions involve "nonsymmetric" clouds. Thus, in a simple but natural way, we are able to begin exploring the role of asymmetry in collisions. Properties of the clouds used in each simulation are summarized in Table 1.

The natural timescale for individual supersonic cloud evolution is the so-called "crushing time," $\tau_{\rm cr}$ (e.g., KMW; Jones, Kang, & Tregillis 1994), defined as

$$\tau_{\rm cr} = \frac{2R_c\chi^{1/2}}{v_c} = \frac{2R_c\chi^{1/2}}{Mc_{\rm si}} = 1.3\left(\frac{R_c}{\rm pc}\right)\left(\frac{\chi}{100}\right)^{1/2} \times \left(\frac{M}{1.5}\right)^{-1}\left(\frac{c_{\rm si}}{10\ {\rm km\ s^{-1}}}\right)^{-1}\ {\rm Myr}\ . \quad (4)$$

During an interval $\tau_{\rm cr}$, a cloud moving through an external medium develops a bow shock and is maximally compressed by an internal shock originating at the front part. An extended, low-pressure wake develops behind the cloud. Also on this timescale, KHIs and RTIs start to disrupt the cloud as it begins to become decelerated with respect to its background (e.g., Vietri, Ferrara, & Miniati 1997). In the absence of magnetic fields, simulations show that clouds disrupt because of instabilities on timescales $t \geq \tau_{\rm cr}$. Detailed discussions of the physics of individual, supersonic cloud evolution may be found in Doroshkevich & Zeldovich (1981), Jones et al. (1994), (1996), Schiano, Christiansen, & Knerr (1995), and Vietri et al. (1997). For the clouds considered here, $\tau_{\rm cr} \sim 5.3 \times 10^5$ yr in the adiabatic case ($R_c = 0.4$ pc), and $\tau_{\rm cr} \sim 2 \times 10^6$ yr in the radiative case ($R_c = 1.5$ pc). These are of the same order as the mean time for a cloud to have a collision in the ISM (Stone 1970a,

TABLE 1

SUMMARY OF TWO-DIMENSIONAL HYDRODYNAMIC CC SIMULATIONS

CASE[a]	η[b]	R_c (pc)	$\tau_{\rm coll} = R_c/v_c$ (yr)	$\tau_{\rm cr} = 2R_c\sqrt{\chi}/v_c$ (yr)	M_r[c]	CLOUDS AGES C1 ($\tau_{\rm cr}$)	CLOUDS AGES C2 ($\tau_{\rm cr}$)	END TIME[d] ($\tau_{\rm coll}$)
1.....	Adiabatic	0.4	2.6×10^4	5.3×10^5	3	0	0	67.5
2.....	0.38	1.5	9.7×10^4	2.0×10^6	3	0	0	37.5
3.....	Adiabatic	0.4	2.6×10^4	5.3×10^5	2.7	1	1	22.5
4.....	0.38	1.5	9.7×10^4	2.0×10^6	2.8	1	1	22.5
5.....	Adiabatic	0.4	2.6×10^4	5.3×10^5	2.4	1	1.5	22.5
6.....	0.38	1.5	9.7×10^4	2.0×10^6	2.7	1	1.5	30.0

[a] All models have used $\gamma = 5/3$, $\chi = \rho_c/\rho_i = 100$, and equilibrium pressure $p_{\rm eq}/k_{\rm B} = 1628$ K cm^{-3}. Also, at equilibrium, we have $T_i = 7400$ K and $n_i = 0.22$ cm^{-3} for the intercloud medium and $T_c = 74$ K and $n_c = 22$ cm^{-3} inside the clouds. Furthermore, all the computations were carried out on a rectangular grid with size $N_X = 2N_Y = 1024$ corresponding to a resolution of 50 zones through the cloud radius. The left, top, and right boundaries are free, whereas reflection is assumed at the bottom.

[b] $\eta = \tau_{\rm rad}/\tau_{\rm coll}$.

[c] This is the *relative* Mach number and is referred to the intercloud sound speed, $c_{\rm si} \simeq 10$ km s^{-1}.

[d] The end time is expressed in terms of collision time $\tau_{\rm coll}$ and represents the total time from the beginning of the collision.

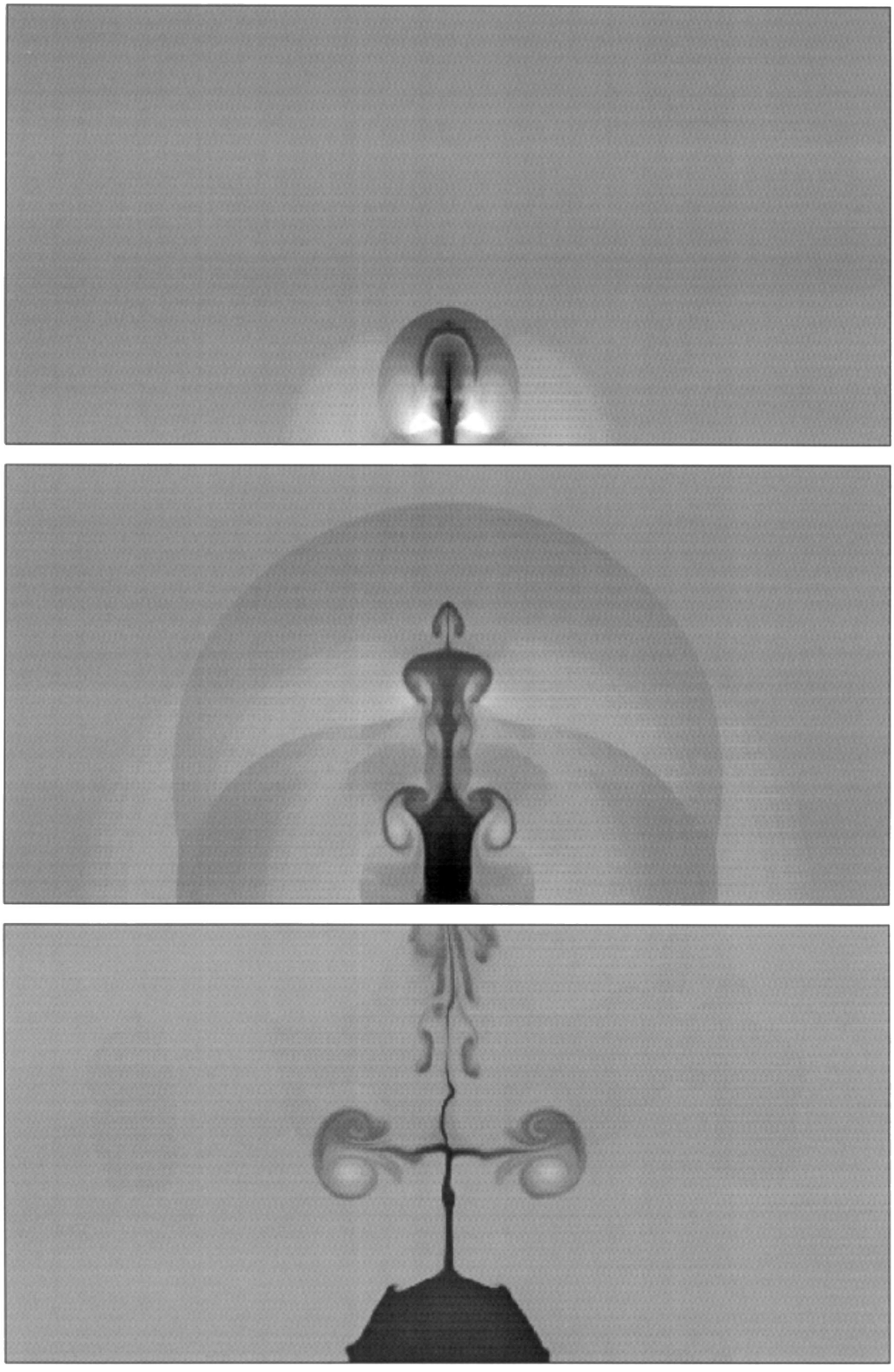

FIG. 3.—Same gray scale as in Fig. 1, but for case 2. *Top*: the compression phase at $t = 1.5\tau_{\rm coll}$ and the ejection of material along the collision plane of the crushed clouds. *Middle*: the reexpansion phase at $t = 3.7\tau_{\rm coll}$; the (slab) jetlike structure is well formed and is showing features common to astrophysical jets. *Bottom*: the structure at $t = 37.5\tau_{\rm coll}$, when the two clouds have merged into a structure with a dense rim. By this time, KHI structures are evident along the jet and on the perimeter of the merged cloud.

1970b; Spitzer 1978; Hausman 1981). This further supports our feeling that cloud evolution prior to the collision must be considered. In our study, we begin the individual cloud evolution at $t = -\tau_{\rm cr}$ for "symmetric, evolved" CCs. For "nonsymmetric, evolved" CCs, one of the clouds begins its evolution at $t = -1.5\tau_{\rm cr}$ before the collision event. For these purposes, we define the collision as beginning (i.e., $t = 0$) when the bow shocks of the two clouds osculate.

3. NUMERICAL SETUP

3.1. *The Code*

We simulate the CC problem using a two-dimensional Eulerian hydrodynamical code on a Cartesian grid. The code we used is based on an explicit total variation diminishing, conservative finite-difference scheme, second-order accurate in both time and space (Harten 1983; Ryu et al. 1993). Multidimensional flows are handled by the Strang-type dimensional splitting (Strang 1968). We accounted for radiative cooling in each time step by explicitly correcting the total energy after updating hydrodynamical quantities.

Radiative losses are described generally by the following equation:

$$\frac{de}{dt} = -\mathscr{L} , \tag{5}$$

where e is the internal energy and $\mathscr{L} = n^2\Lambda(n, T) - n\Gamma$ accounts for the net loss to radiation against nonadiabatic heating. The cooling term $\mathscr{L}$ defines the cooling timescale

$$\tau_{\rm rad} = \frac{e}{\mathscr{L}} . \tag{6}$$

When radiative losses are very high, as they can be during the compression phase, the cooling timescale, $\tau_{\rm rad}$, is comparable to or less than the dynamical timescale that, by the Courant condition, ordinarily determines the computational time step. In this case, the cooling term is labeled "stiff." There are several ways to handle stiff cooling terms (see, e.g., LeVeque 1997). One way is to choose the shorter of $\tau_{\rm rad}$ and the time step imposed by the Courant condition as the computational time step. However, in some situations, this choice may lead to uncomfortably short computational time steps. On the other hand, we could employ Strang's operator splitting approach, where the cooling is computed by multiple steps with its own time step, during one computational time step determined by the Courant condition. We chose a third approach in which equation (5) is rewritten as

$$\frac{d\ln(e)}{dt} = -\frac{\mathscr{L}}{e} = -\frac{1}{\tau_{\rm rad}} . \tag{7}$$

This leads to the solution between time steps j and $j + 1$,

$$e^{j+1} = e^j \exp\left(-\frac{\mathscr{L}\Delta t}{e^{j+1/2}}\right). \tag{8}$$

For this method, the cooling is computed in a single step even though the cooling timescale is smaller than the dynamical timescale. The method ensures that the internal energy is always positive, with the computational time step, Δt, determined by the Courant condition. If one uses the initial value e^j for $e^{j+1/2}$, however, the radiative correction is only first-order accurate in time. The radiative cooling function we used, $\Lambda(n, T)$, includes free-free emission, recombination lines, as well as collisional excitation lines with a standard solar metallicity ($Z = Z_\odot$), whereas the heating (Γ) is provided through ionization and photoionization processes and by cosmic rays (for a full description, see Ferrara & Field 1994). We have neglected the effects due to dust grains considered by RFM; this accounts for the slight difference in the ISM phase properties of our model with respect to theirs.

To allow tracking of material that was initially identified with each of the clouds, we introduced a passive tracer, S, usually referred to as "color" (Xu & Stone 1995). This quantity (actually one for each cloud) is initially set to unity inside each cloud and zero elsewhere. It represents the fraction of material inside each cell that was originally part of one of the clouds. The evolution of the color is followed with van Leer's second-order advection scheme (van Leer 1976).

3.2. *Grid, Boundary Conditions, and Tests*

In each simulation, the clouds are centered on the X-axis with reflection symmetry assumed across this axis. Only the plane $Y \geq 0$ is included in the computational box. Tests with this code show that this more economical grid gives results equivalent to those obtained with a full plane. The length scale is adjusted for each case so that $R_c = 1.0$. In those units, the computational domain is $X = [0, 20]$ and $Y = [0, 10]$. The grid is Cartesian, so that our clouds are actually cylinders. The left, top, and right boundaries are open. Reflections at these open boundaries are too small and too far away from the collision to affect the structure of the flow. Test calculations with a computational box twice as large show no relevant differences from the results we describe below. We have explored a range of numerical resolutions, although only the computations at the highest resolution are presented here. These involve a 1024×512 grid, which provides a resolution of 50 zones across the initial cloud radius. We have also compared our results on a uniform 512×256 grid with the Adaptive Mesh Refinement hydrodynamics results of KMW. Our simulations are purely hydrodynamical, while they added, for convenience, a magnetic pressure (but no other magnetic effects) to limit compression behind radiative shocks. Still, for the same parameters, we obtain results consistent with theirs in terms of main hydrodynamical feature development.

3.3. *Numerical Values, Physical Parameters, and Initial Conditions*

The parameters involved in the problem are quite numerous, and a comprehensive study is beyond our present scope. However, since we are interested in assessing the importance of radiative losses, the preevolution of clouds through the intercloud medium, and the symmetry of the problem, we have decided to restrict as much as possible the parameters' space by developing an accurate model for the multiphase structure of the ISM, in agreement with observational data. We then adopt the most typical values for cloud and WIM physical properties as derived from such a model, hoping that they are truly representative of the ISM conditions. In the following, we give an outline of model assumption.

As mentioned in § 2, we consider clouds that are initially uniform and in pressure equilibrium with the intercloud medium. We set the initial density contrast $\chi = n_c/n_i = 100$, where n_c and n_i are the cloud and intercloud number densities, respectively, and $n_c = 22$ cm^{-3} ($\Rightarrow n_i = 0.22$ cm^{-3}); the cloud temperature is $T_c = 74$ K ($\Rightarrow T_i = 7400$ K). This particular choice is dictated by the radiative cooling function adopted in our calculation, by the pressure equilibrium assumption, and by the density contrast between the two different phases. The equilibrium thermal pressure for the ISM turns out to be $p_{\rm eq}/k_{\rm B} = 1628$ K cm^{-3}. Each cloud has an initial Mach number $M = v_c/c_{\rm si} = 1.5$, where $c_{\rm si}$ is the sound speed in the intercloud medium. The adiabatic index $\gamma = 5/3$ [$p = (\gamma - 1)e$] is assumed throughout the calculations. For the adiabatic cases, we set $R_c = 0.4$ pc, whereas

for the radiative ones, $R_c = 1.5$ pc. With this choice of the parameters, we have $c_{si} \approx 10$ km s^{-1} and $v_c \approx 15$ km s^{-1}; $\tau_{coll} \approx 2.6 \times 10^4$ yr for the adiabatic cases. For the radiative cases, $\tau_{coll} \approx 9.7 \times 10^4$ yr, and the radiative cooling time inside the clouds turns out to be $\tau_{rad} \approx 3.7 \times 10^4$ yr, yielding $\eta \approx 0.38$. Finally, the Jeans length associated with the initial clouds is $\lambda_J \approx 29$ pc $\gg R_c$. In the radiative symmetric collisions, the large density increase produced during the compression phase causes a significant reduction of λ_J, which becomes comparable to, yet still larger than, the vertical size of the clouds. For this reason, we have neglected self-gravity throughout our calculations (see also KMW). However, in a more refined calculation, which would take into account other processes like chemical reactions or recombination processes, a larger compression might be allowed, making the colliding clouds gravitationally unstable as a result.

As explained in § 2, we have allowed the described adiabatic and radiative clouds to collide under three different circumstances. For cases 1 and 2 in Table 1, uniform clouds are placed on the grid in such a way that their initial boundaries are only two zones apart at $t = 0.0$. These are the so-called "nonevolved" cases. For cases 3 and 4, each cloud begins an independent evolution at $t = -\tau_{cr}$ (as appropriately determined by their properties listed in Table 1). In these cases, $t = 0.0$ is defined as the moment when the bow shocks of the clouds osculate. For cases 5 and 6, one of the clouds begins its independent evolution earlier, at $t = -1.5\tau_{cr}$. Again, the two clouds' bow shocks come together at $t = 0.0$. Table 1 lists these details. Animations of each simulation have been posted on the World Wide Web site at the University of Minnesota.

4. RESULTS

4.1. *Collision of Nonevolved Clouds*

Figure 1 shows the four phases defined in § 2 for an adiabatic collision (case 1). At the earliest time shown (Fig. 1*a* [*top panel*]), $t = 1.5\tau_{coll}$, the collision is near the end of the compression phase. At the very beginning of this phase, a one-dimensional analysis in the limit of a strong shock can still be applied to the shocks propagating through the clouds. Theory predicts $\rho \sim 4\rho_c$ and $p \sim (4/3)\rho_c v_c^2$, in very good agreement with the numerical values found (Fig. 2). The high pressure in the interaction region limits the compression and leads to a fast reexpansion. The compression phase lasts longer near the cloud centers, because the cloud column density is maximum along $Y = 0$ and because some gas is vertically squirted out from side edges of the interaction region, right after the beginning of the collision (Fig. 1*a* [*top panel*]). The ejected material propagates through the lower density WIM and, later on, develops features commonly seen in astrophysical jets. In particular, this slab-jet structure shows a working surface bounded by a shock, a cocoon surrounding the jet, and apparent KHIs. Nevertheless, since this gas represents a small fraction of the total mass of the clouds, it does not affect the development of the collision very much. At the end of this phase, the gas is highly compressed into a layer much thinner than the initial cloud size (Fig. 1*a* [*top panel*] and Fig. 2).

After $t = 1.5\tau_{coll}$, as already pointed out in § 2, the shocks generated within the clouds during the collision enter the WIM and allow the clouds to reexpand. Reexpansion takes place supersonically, generating a shock that, with the jet shock, develops a nearly circularly expanding shock structure on the X-Y plane. Inside this structure, a reverse shock is generated, and the reexpanding cloud material begins to accumulate in a dense shell with $\rho \sim 30\rho_i$ (Fig. 2). By $t = 8.2\tau_{coll}$ (Fig. 1*a* [*bottom panel*]), a dense layer is well formed and, despite its expansion, has become the region of highest density ($\rho \sim 10$–$16\rho_i$). It has a nearly circular shape, except for distortions by KHIs and RTIs, which eventually form long dense ($\rho \sim 11.5\rho_i$) fingers. The shell expands at pretty high velocity ($v \sim 1.1c_{si}$). After about $t = 12\tau_{coll}$, the reexpansion of the shell halts, just before the reverse shock passes from the shell into the central low-density cavity. Then the collapse of the shell begins. Figure 1*b* (*top panel*) shows the collapse phase at $t = 37.5\tau_{coll}$. Eventually, the reverse shock reflects off the X-axis and rebounds. But it is then largely disrupted by refraction in the irregular density structure of the collapsing cloud material. Large-scale vortices are generated that, through KHIs and RTIs, hasten the formation of complex filaments evident by $t \sim 67.5\tau_{coll}$ (Fig. 1*b* [*bottom panel*]). At the end of the simulation, what remains of the two clouds is a very low density central region, with ρ mainly between 2 and $3.5\rho_i$ (Fig. 2), surrounded by a complex of filaments, which are mixing the original cloud material with the WIM. *We deduce that, in case 1, the likely fate of the clouds is disruption and conversion of cloud material into the WIM phase.*

The analogous radiative case 2 is shown in Figure 3. During the compression phase (Fig. 3, *top panel*), a fair fraction of the thermal energy is radiated away (Fig. 9 below). As a consequence, the density reaches very high values ($\rho \sim 10^4\rho_i$), and reexpansion is much slower than in case 1. Since the reexpansion is so slow now, the reverse shock promptly penetrates all the way back to the impact surface and is reflected outward again. This sequence, much like what happens inside a young supernova remnant (e.g., Dohm-Palmer & Jones 1996), eliminates the central low-pressure region. Following this, a significant reexpansion along the initial direction of motion gives back to the merged cloud material a typical cloudlike aspect ratio. The structure undergoes some vertical expansion too, but the most prominent feature in this direction is a thin jet propagating along the symmetry plane of the collision. This is shown in Figure 3. At $t = 9\tau_{coll}$ (Fig. 3, *middle panel*), almost all the cloud gas is still in a core with high density ($\rho \sim 580\rho_i$), surrounded by lower density material with ρ ranging between 200 and $450\rho_i$, and expanding at a very low speed. A comparison of the middle panel of Figure 3 with Figure 1*a* (*bottom panel*) shows clearly that the size of the reexpanded cloud is much larger in the adiabatic case than in the radiative one. As a consequence, in the radiative case, the slab-jet structure is much more distinct. For case 2, the simulation ends at $t = 37.5\tau_{coll}$. *We deduce that, in case 2, the likely fate of clouds is coalescence.* The apparently coalesced clouds have evolved into an almost circular object of radius $\sim 2R_c$ with densities ranging between about $20\rho_i$ in the inner part and $70\rho_i$ at the surface. Its total mass is $M_{tot} \simeq 0.84 \times 2M_c$, where M_c is the initial cloud mass, showing a high efficiency (84%) for the buildup mass mechanism. The edge of the newly formed object is sharply bounded but shows clear signs of KHIs. However, because of the high density of its external layer, KHIs will become effective on a timescale much longer than in the adiabatic case. The expansion velocity inside the merged cloud at the end is small, namely, a few times $10^{-2}c_{si}$. The net radiative cooling

is positive (which means on balance that the gas is losing thermal energy) in the outer, denser part of the merged clouds and negative (which means that the gas is being heated up by the background radiation and cosmic rays) in the inner, more diffuse region, although in both cases the energy gains or losses are not very significant. There is a small outward-facing pressure gradient within the cloud concentration, and so eventual collapse seems likely. Although coalescence seems likely in the near term, the final fate of the cloud is unclear. KMW suggest that the cloud will expand and contract multiple times until pressure and thermal equilibrium are reached, developing filamentary structures along the X-axis in the process. It might also be possible that the lower pressure inside the cloud induces contraction, followed by a sufficient increase in the density to turn the cooling function positive. In that case, the extra pressure due to infall could be radiated away, and the original cloud density, for which radiative equilibrium holds, might be approached. In addition, because of the highly dense external layer around the newly formed structure, we do not expect in the radiative case that RTIs will be as disruptive during the collapse phase as they were in the adiabatic case.

4.2. *Collision of Evolved Clouds: Symmetric Cases*

The top panel of Figure 4 shows the initial conditions for the adiabatic collision of two evolved clouds (case 3). At $t = 0$, when the cloud bow shocks just touch and each cloud has evolved through one crushing time, the density changes smoothly through the clouds, ranging from $10\rho_i$ at the back to $150\rho_i$ at the front part. The X-component of the velocity follows the same pattern, being higher at the front of the cloud than at the rear, although the range of this variable is much smaller (e.g., Jones et al. 1994). On average, the clouds have an individual speed corresponding to a Mach number, $M = 1.35$, relative to the WIM. There are a number of differences introduced into the interaction between the clouds by allowing for prior evolution. The most important are the presence of bow shocks and incoming gas motions within each cloud wake once the clouds collide. After the approaching clouds encounter each other's bow shock, reverse shocks (which act as secondary bow shocks) are generated. In the adiabatic interaction (case 3), these shocks affect the clouds substantially. In fact, at $t = 2.2\tau_{\rm coll}$, right before the cloud bodies encounter the bow shocks, their X-width $l \sim 1.5R_c$ (measured on the X-axis), and $\rho_{\rm max} \sim 150\hat{\rho}_i$, but at $t = 3\tau_{\rm coll}$, after the bow shock–cloud collision begins, $\rho \sim 250\rho_i$ ($\rho_{\rm max} \sim 260\rho_i$), and $l \sim 1.2R_c$. There is further compression so that at $t \sim 3.8\tau_{\rm coll}$, right before the cloud bodies impact each other, $\rho \sim 380\rho_i$ in the compressed front layer, and $l \sim R_c$ (Fig. 4, *middle panel*). So the maximum compression reached during the collision ($t \sim 4.5\tau_{\rm coll}$) ($\rho_{\rm max} \sim 1200\rho_i$) is much higher in case 3 than in case 1, although the pressure enhancement is about the same, and both collisions are adiabatic. If the clouds were self-gravitating, such differences might become important to the possibility for triggering star formation out of such collisions. On the other hand, the jetlike and the thin shell structures develop in roughly the same pattern as for case 1. By comparison with the nonevolved collision, however, more cloud material remains in a core structure, almost to the reexpansion phase. This is evident in Figure 1*a* (*bottom panel*), at $t = 11.2\tau_{\rm coll}$, when contrasted with the bottom panel of Figure 4. The same comparison also shows that the shell structure in case 3 is more irregular than in case 1. This is in fact due to the lower density of the shell in case 3, which allows a quicker development of RTIs and KHIs. By the time shown in Figure 1*b* (*top panel*), expansion along the X-axis has been reduced compared with the Y-direction. That results from the interaction between the expanding cloud material and the inflowing WIM within the wakes of the two clouds. The ram pressure of the wake flows is strong enough to affect significantly the expansion along this path. Indeed, at $t \sim 15\tau_{\rm coll}$, a standing reverse shock is well formed and deflects the expanding cloud material away from the X-axis. This in turn becomes strongly sheared and filamentary because of KHIs. A substantial fraction of the cloud material is ejected so that it cannot join the collapse. The shock structures in this case are very complex, since they involve interactions with the preexisting bow shocks and tail shocks and a generally more complex density and pressure structure as the collision begins. Nevertheless, as our simulation of case 3 ends ($t = 22.5\tau_{\rm coll}$), the dominant, irregular shell structure resembles qualitatively that in case 1. Subsequent evolution in case 3 should follow a pattern similar to that in the analogous nonevolved case 1. *In particular, we expect disruption of the clouds in both cases.*

In the radiative evolved case (case 4), the individual clouds show a similar qualitative structure to those in case 3, but now their compression due to initial motion through the intercloud medium is much higher ($\rho_{\rm max} \sim 1400\rho_i$). The additional compression results from enhanced radiative cooling induced by the shock compression within the cloud. We note that the bow shock compression phase that was important to case 3 turns out not to produce a very significant effect for case 4. This is true for the following reason: the compression brought on by radiative losses prior to the encounter is already very large. In addition, since the speed at which the bow shock penetrates each cloud scales inversely with the square root of density, in this case the bow shocks barely penetrate into the clouds' bodies before they collide, producing only little precompression with respect to the adiabatic case. As a result, the compression reached during the collision is only slightly higher ($\rho_{\rm max} \sim 4 \times 10^4\rho_i$) than in the nonevolved case (case 2). The reexpansion phase in case 4 follows pretty much the same pattern as in case 2, except that now it is substantially slowed down in some directions by the action of the wakes behind each cloud, as we noted also for case 3. In fact, as shown in Figure 5, by the end of this simulation ($t = 22.5\tau_{\rm coll}$), the clouds have merged into a dense structure of size $\sim 2R_c$, which is $\frac{2}{3}$ of the size of the merged core in case 2. Expansion in the Y-direction is relatively free and leads to a Kelvin-Helmholtz unstable jet, as in the other symmetric collisions. However, reexpansion along the X-axis is strongly inhibited by inflowing wake material, so that the velocity of expansion along the X-axis is only about $\frac{1}{3}$ as large compared with case 1. As a result the expanding gas collects in a high-density cloud "rim" ($\rho \sim 400\rho_i$, $\rho_{\rm max} \sim 440\rho_i$). The wake material forms a standing, outward-facing, "accretion shock" outside the cloud structure. Examination of the color variable shows a very good correspondence between the high-density material visible in Figure 5 and the cloud material. Thus, the figure shows that wake material, once it impinges on the cloud, joins the outflow of cloud material in the Y-direction. In fact, it appears that the inflowing wake material and associated shocks are responsible for driving the vertical outflow of cloud material along the jet and for

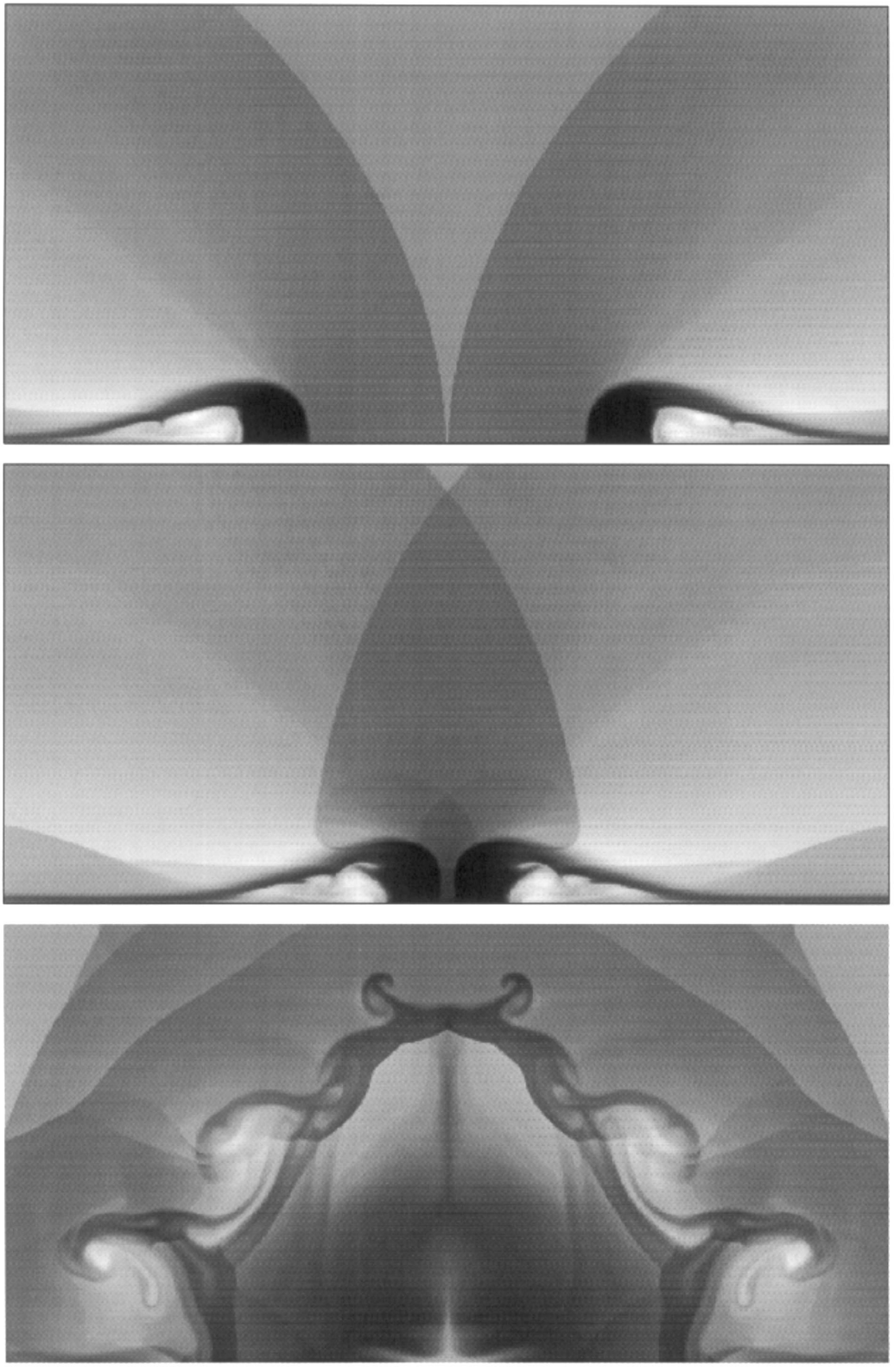

FIG. 4.—Same gray scale as in Fig. 1, but now for case 3. *Top*: conditions when the bow shocks generated by the clouds osculate, just prior to impact. *Middle*: the two clouds a little before the actual cloud-body collision. The clouds have been compressed by the bow shocks. *Bottom*: the reexpansion phase at $t = 11.2\tau_{\rm coll}$. The two clouds are still distinguishable; also, a low-density layer has formed around them and is undergoing strong ablation by KHIs.

producing the KHIs that have generated the large eddies evident in Figure 5. In the inner cloud, the density ranges between 100 and $200\rho_i$, which is higher by almost a factor 2 with respect to the nonevolved case. Even though there is a weak pressure gradient pushing vertically in the central condensation, it seems very likely that in an extension of this simulation, the main core of the merged clouds would remain intact. *So we judge these clouds to be coalesced.*

4.3. *Collision of Evolved Clouds: Asymmetric Cases*

As mentioned earlier, we chose a simple but natural way to explore symmetry breaking in the collisions just dis-

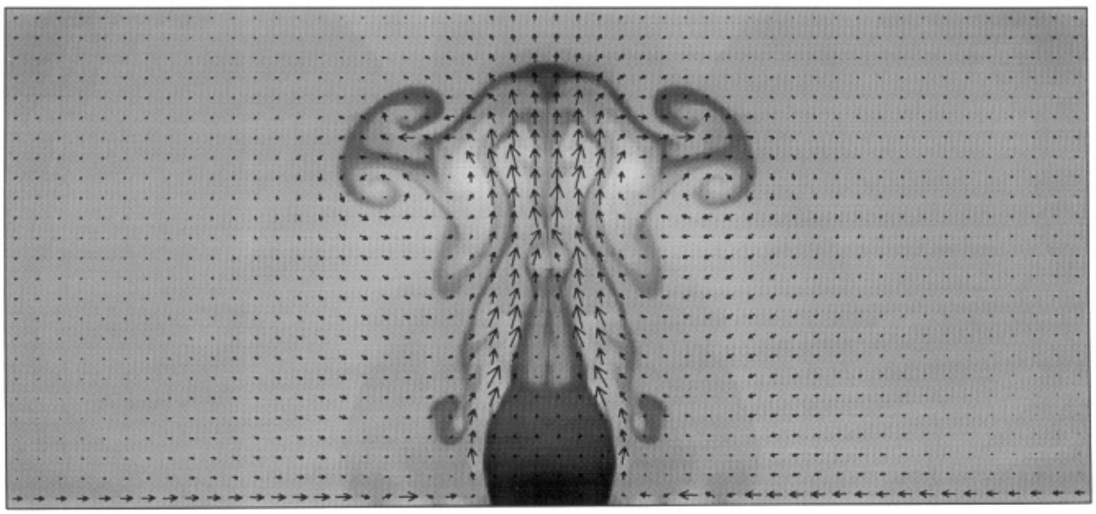

FIG. 5.—Same gray scale as in Fig. 1, but now for case 4, with velocity vectors superimposed. This image shows the final stage of the reexpansion at $t = 22.5\tau_{\rm coll}$. The two clouds have merged into a new structure with density decreasing from the bottom to the top. Delicate density features have been produced by KHIs, enhanced by inflowing wake material deflected along the sides of the clouds.

cussed. That is, we collided clouds that were identical when set into motion but that were evolved differently at impact. On a timescale $\sim\tau_{\rm cr}$, the compression deforms the clouds substantially, while KHIs and RTIs will produce irregular cloud boundaries. Since those features are highly time dependent, two clouds of even slightly different dynamical ages will lack mirror symmetry. In our asymmetric simulations, one cloud (hereafter C1) was aged by $1\tau_{\rm cr}$ and the other (hereafter C2) by $1.5\tau_{\rm cr}$ as their bow shocks came in contact at $t = 0.0$. In general, the older cloud had a denser front part and a smaller velocity at impact (Jones et al. 1994). However, the aspect ratio (length-to-height ratio) developed by the cloud during its motion through the WIM is strongly related to the adiabaticity of the gas. Indeed, it decreases in the adiabatic case but increases in the radiative one, so that the radiative cloud grows denser and more compact as it evolves (Vietri et al. 1997). This turns out to have a major impact on the survival of clouds in asymmetric CCs. As in the previous evolved cases, the two clouds undergo bow shock compression before colliding bodily. In the asymmetric interactions, the clouds have different speeds and shapes and are located at different distances from their bow shocks. As a result, they no longer experience compression simultaneously. In addition, since C2's bow shock is weaker than C1's, bow shock compression for C2 turns out to be stronger than for C1. In the adiabatic case 5, right before the direct collision, C1 has $\rho \sim 300\rho_i$ and $l \sim R_c$, and C2 has $\rho \sim 370\rho_i$ and $l \sim 0.6R_c$. The compression phase is shorter than in cases 1–4, and not all of the kinetic energy is converted into thermal energy (Fig. 8 below). After the collision, the younger, more compact cloud, C1, maintains its identity longer than C2. As shown in Figure 6, at $t = 8.2\tau_{\rm coll}$, C1 still has a dense core with $\rho \sim 70\rho_i$ surrounded by a layer with $\rho \sim 40\rho_i$. By contrast, C2 is being stretched and torn apart and, soon after, is mostly converted into the WIM. Nevertheless, C1 is undergoing rapid reexpansion also, and at $t = 13.5\tau_{\rm coll}$, the density is lower than $15\rho_i$ everywhere. Although it is much more irregular than cases 1 or 3, in case 5 we can still recognize a clear pattern in the evolution of the reexpansion

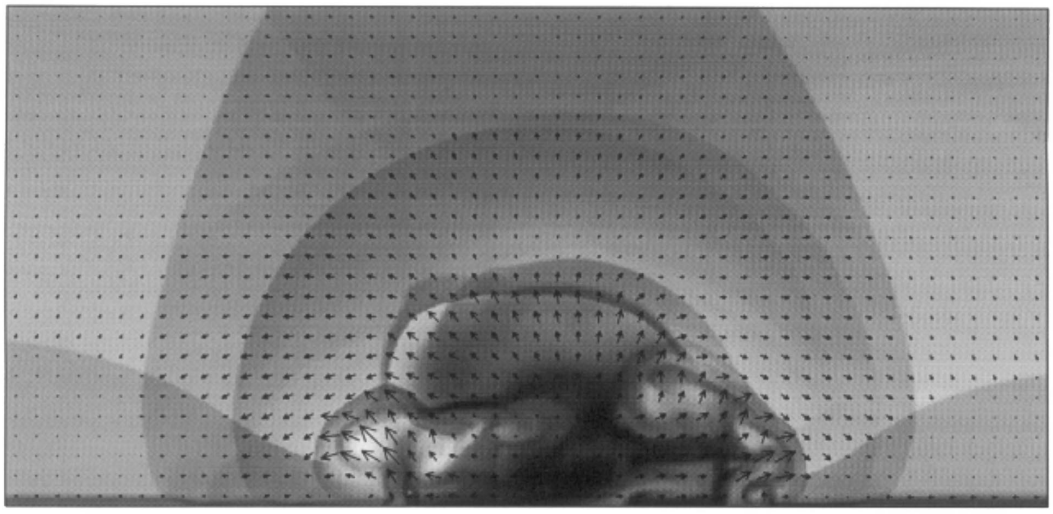

FIG. 6.—Same gray scale as in Fig. 1, but now for case 5, with velocity vectors superimposed. This image shows the complicated reexpansion phase at $t = 8.2\tau_{\rm coll}$. The cloud originating on the left (C1) is still recognizable, whereas C2, coming from the right, has been strongly distorted from its original form.

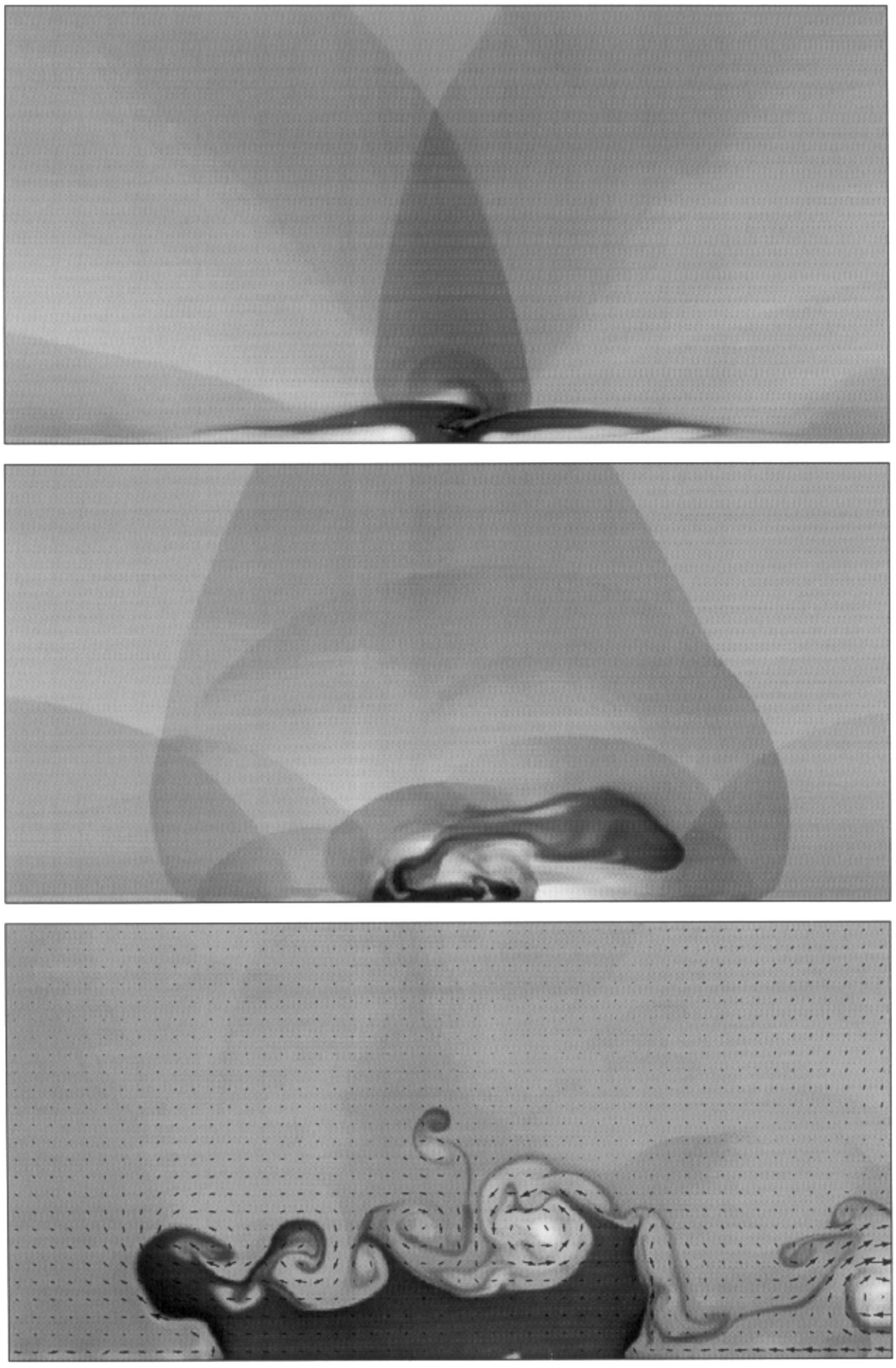

FIG. 7.—Same gray scale as in Fig. 1, but now for case 6. *Top*: the compression phase at $t = 3.7\tau_{\rm coll}$. The contact surface is quite irregular and asymmetric, foretelling of the disruption to follow. *Middle*: the structure at $t = 9\tau_{\rm coll}$ showing the formation of a cloudlet breaking off from C1. *Bottom*: density with superimposed velocity vectors, representing the reexpansion phase at $t = 30\tau_{\rm coll}$. A large irregular structure has formed, and eddies are shredding the top part.

phase, with the formation of an expanding shock wave, along with a reverse shock and a low-density shell, heavily affected by KHIs and RTIs. So, at the end of the second reexpansion phase, part of the cloud gas has already been converted into the WIM, whereas the remaining part is forming an irregular filamentary structure with ρ ranging between 5 and $10\rho_i$. As in the symmetric-evolved collisions, the interaction between reexpanding cloud material and

inflowing wake gas influences the expansion significantly. As for case 3, the wake confines expansion along the X-axis through a standing, inward-facing shock. Also, as in case 3, the expanding cloud material is deflected around the wake in a strongly sheared manner. The broken symmetry in case 5 allows C2 material to expand much more easily, however, because its greater Y-extent at impact effectively "launches" it over the wake of C1. In addition, since C2 has a lower column density just above the X-axis, it recoils in response to the collision. Thus, a substantial fraction of C2 passes over its own wake after the collision. Those effects add considerably to the disruption of cloud material into filaments and probably hasten its dispersal into the WIM. The resulting flow is very complex and highly vortical. So we expect the collapse phase to be very ineffective at collecting material into new clouds. *Thus, this case clearly seems much more disruptive than any of the previous ones.*

On the other hand, the radiative case 6 is characterized by completely new features. At $t = 2.2\tau_{\rm coll}$, the region between the two shocks formed by the collision appears to be strongly distorted, resembling the structure that develops during the "bending mode instability" (KMW; Vishniac 1994; Hunter et al. 1986). As shown in the top panel of Figure 7, at $t = 3\tau_{\rm coll}$, the layer between the two shocks has grown more corrugated, and the front parts of the clouds are following the same pattern. Although the bending mode is unstable, the disruption of the impact surface is due primarily to the gross irregularities of clouds' shape, which dominate the determination of the evolution of the structure of the flow. The top panel of Figure 7 also shows that the upper part of the left (C1) cloud is about to break off and pass over the other cloud (C2), carrying some of C2's gas with it. As already pointed out, unlike the adiabatic case, in the radiative case the older cloud, C2, has a more compact structure, which makes it more solid and more resistant to the collision than C1. At $t = 9\tau_{\rm coll}$ (Fig. 7, *middle panel*), the material from C1 passing over the top of C2 has expanded again into a distinct cloudlet, with density ranging from $\rho \sim 100\rho_i$ at the front to $\rho \sim 5\rho_i$ at the tail, and with still slightly supersonic velocity ($v_X \geq c_{\rm si}$). Subsequently, that cloudlet becomes strongly decelerated and suffers KHI- and RTI-induced destruction, as seen previously for individual clouds (e.g., Jones et al. 1994). Although the cloudlet leaves our grid before it is destroyed, it seems fairly clear that it will dissolve into the WIM. The wake of the cloudlet is still visible on the far right-hand side in the bottom panel of Figure 7. On the other hand, the core of C2, which, by $t = 3\tau_{\rm coll}$, has a very long tail and a dense but distorted front, passes through the remaining part of C1, emerging after $t \approx 7.5\tau_{\rm coll}$ with the main body of C2 accreted. This outcome resembles those that one would expect in collisions of two clouds of quite different sizes and densities. It shows that the smaller and denser cloud is able to pass through the larger and more diffuse one, sweeping its gas and finally breaking it up into two major pieces (Gilden 1984; Kimura & Tosa 1996). In these calculations, we show that the same fate can actually occur when two clouds with approximately the same initial characteristics but with slightly different morphologies collide.

As in the other collisions between clouds that are followed by wakes, an "accretion" shock forms to the right of C2. However, it is driven off the grid to the right before the simulation ends. The interaction is dominated in this case by the high concentration of material in C1.

The merged remnant of C1 and C2 that was formed by $t = 7.5\tau_{\rm coll}$ has by the end of the simulation, $t = 30\tau_{\rm coll}$, evolved into nonuniform filamentary structures, characterized by irregular motion (Fig. 7, *bottom panel*). Very little mixing between the two original clouds has actually taken place; rather, one has passed through the other. On the other hand, considerable entrainment of WIM gas has taken place through the action of eddies generated during the collision. The higher density features apparent on the left and top perimeter of the main cloud visible in the bottom panel of Figure 7 are, in fact, the remnant merged cores of the original clouds, whereas the rest of the main cloud at this late time contains a strong mix of entrained material or has been ejected from the grid. At this time, the main cloud is being slowly stretched along the X-axis ($v_X \sim 0.1c_{\rm si}$ at the edges), while large eddies on the top and downward-pointing pressure forces are effective at reducing its height. It seems likely that the single dense region visible in the bottom panel of Figure 7 will be bisected into two before too long. The final outcome may be two distinct clouds formed largely from material originally in C2, which was the more compact of the original pair. Thus, the outcome is completely different from that of cases 2 and 4, and *we conclude that the two clouds are destroyed by the collision and converted into several filamentary structures.*

5. DISCUSSION

For the six cases summarized in Table 1, we have investigated the collision of diffuse H I clouds in a multiphase medium. Our objective is to understand such issues as the likely fate of clouds after collisions, including the conditions for coalescence and the fraction of the initial kinetic energy radiated away. In the previous section, we outlined the basic dynamical evolution of each collision and the ultimate fate of the clouds. It was clear from those examples that the fate of colliding clouds depends strongly on the symmetry of the interaction and also on the degree to which the initial kinetic energy is radiated away before the clouds begin their reexpansion. To clarify and expand on those issues, we now review the main points separately for the adiabatic and radiative cases.

5.1. *Adiabatic Cases*

Adiabatic collisions generally appear to result in cloud disruption, with most of the gas converted into the WIM phase. This point is made clearer in Figure 8, which shows a plot of various properties characterizing individual clouds involved in adiabatic collisions. In particular, using the color variables, we can follow the kinetic and thermal energies of each cloud, normalized to the initial cloud total energy, as well as the center-of-mass coordinates $X_{\rm cm}$ and $Y_{\rm cm}$ for each cloud relative to the point of first contact (see Jones et al. 1996 for a mathematical definition of $X_{\rm cm}$ and $Y_{\rm cm}$). From a comparison of the left panels in Figure 8, we see that in all adiabatic cases, 1, 3, and 5, the kinetic energy of the clouds $E_{\rm kin} = 1/2M_c v_c^2$ is initially converted mostly into thermal energy $E_{\rm ther} = pV/(\gamma - 1)$ during the compression phase, through the action of the main outward-moving shocks as they pass through the cloud bodies. That stage is immediate for the "nonevolved" collision but is delayed, of course, for the "evolved" cases, since $t = 0$ corresponds to the moment when the bow shocks touch rather than to the moment when the clouds first touch. During the reexpansion phase, some of this thermal energy is converted back

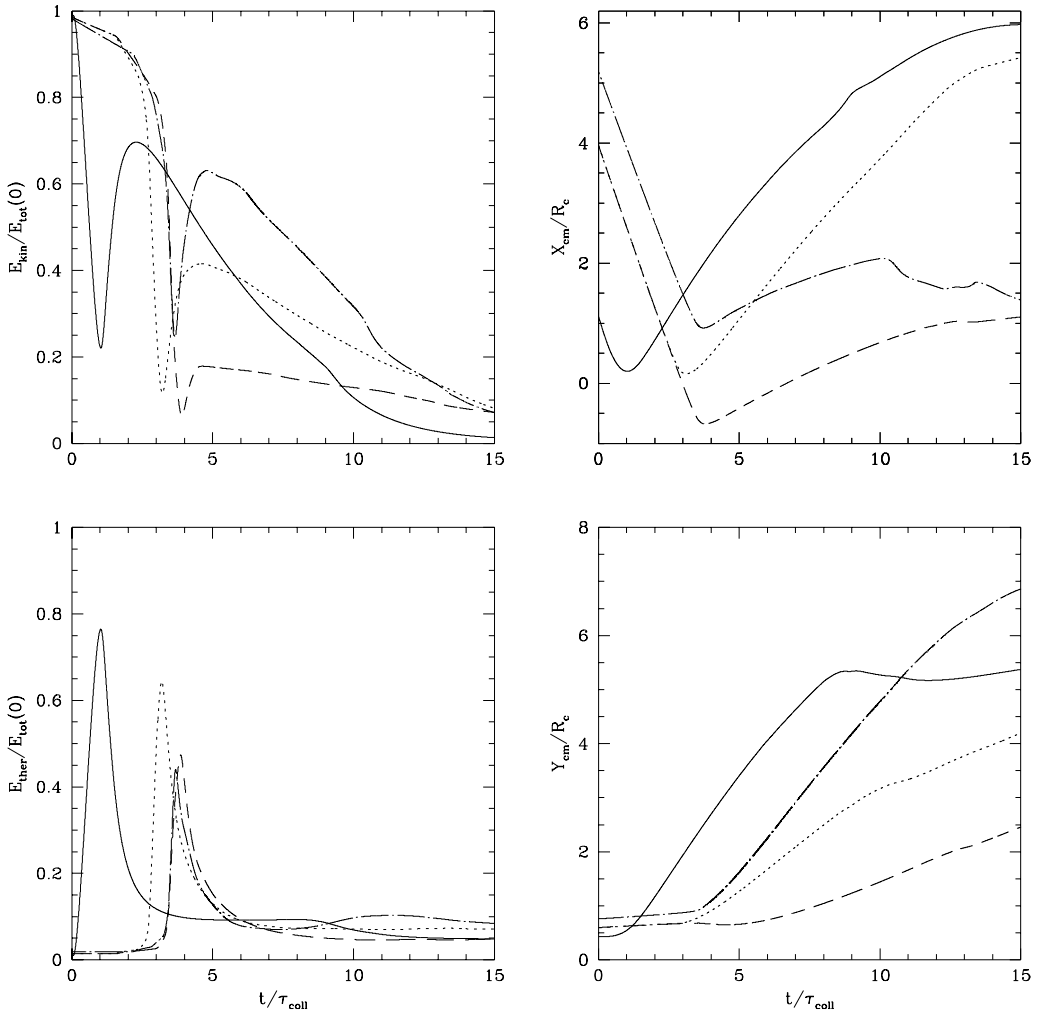

FIG. 8.—Adiabatic cases. The four panels show plots of the kinetic energy (*top left*), thermal energy (*bottom left*), and center-of-mass X_{cm} (*top right*) and Y_{cm} coordinates (*bottom right*), as a function of time, for each cloud involved in the collision. For cases 1 and 3, the two colliding clouds are identical to each other, and so only one is displayed in each case. The solid lines correspond to case 1, the dotted lines to case 3, the dashed and dot-dashed lines, respectively, to C1 and C2 in case 5. The delay of the features of cases 3 and 5 with respect to the nonevolved case 1 is due to the delay in the former cases between the impact of bow shocks and cloud bodies.

into kinetic form, since the rapid expansion of the "blast wave" into the WIM reduces the pressure around the merged clouds. But because the cloud shocks have generated entropy, the cloud gas has substantially more thermal energy at the end of each simulation than at the start, despite considerable volume expansion. This effect enhances the tendency for the cloud material to be converted into the WIM phase following the collision. Also, these plots show that the normalized kinetic energy decreases gradually with time; this is due to the irreversible work done by the expanding gas on the surrounding background. A similar trend was observed in the three-dimensional simulations of two colliding gas streams by Lee, Kang, & Ryu (1996). It is important to note that at late times ($t \geq 8\tau_{coll}$) some energy decrease is also due to the escape of matter from the computational domain, particularly the top. The center-of-mass positions provide a quantitative measure of this expansion, as shown in the right panels of Figure 8. In particular, note for case 1 that the maximum in Y_{cm} around $t \geq 8\tau_{coll}$ corresponds to the time when the dense shell reaches the top of the grid. After that time, Y_{cm} represents the only mass remaining within the grid. The top right panel of Figure 8 also illustrates quantitatively how cloud material in the symmetric collisions is more efficiently removed from the central interaction region than it is in the asymmetric case. Notice for case 5 that some cloud material remained in the interaction region interior. In bottom right panel of Figure 8, we also see the clear difference in Y-expansion of the individual clouds in the asymmetric case 5. The more evolved cloud, C2, that begins the simulation, having a greater height and lower column density along central impact axis, is obviously disrupted by this measure. On the other hand, the more compact cloud, C1, remains compact in this dimension.

5.2. *Radiative Cases*

In the radiative cases, as long as the initial geometry is symmetric, the two colliding clouds merge, and it seems likely that the conditions do exist for a new massive cloud to form. As shown in Figure 9, the kinetic energy of the two clouds is converted into thermal energy and soon radiated away. Indeed, unlike the adiabatic cases, after the compression phase there is no reenhancement of the kinetic energy, as is shown by a comparison of the right panels in Figures 8

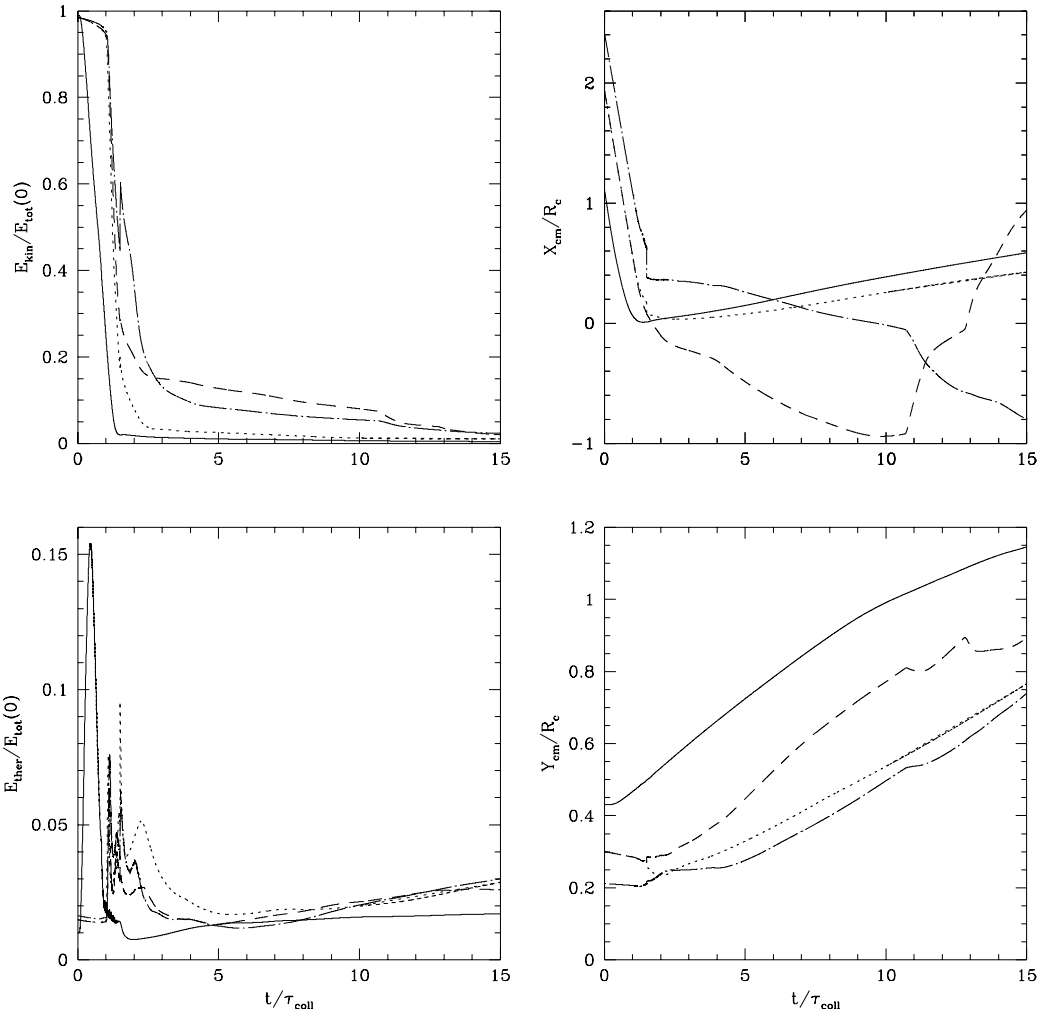

FIG. 9.—Radiative cases. Same as in Fig. 8, but now the solid lines refer to case 2, the dotted lines to case 4, the dashed and dot-dashed lines, respectively, to cloud C1 and C2 in case 6. Taking care to note the significant difference in the Y-axis scale, a comparison with the left panels of Fig. 8 shows that in the radiative cases, much less kinetic energy is converted into thermal form. In addition, as shown by the X_{cm} and Y_{cm} panels (*right*) and by the significant difference in the Y-axis scales of the two figures, reexpansion is much reduced.

and 9. As a result, the reexpansion of the gas is much reduced with respect to the adiabatic case. At the end of the evolution, the thermal energy of the clouds has increased, because of heating processes occurring during the reexpansion phase (Fig. 9). Also, in the evolved (symmetric) cases, the density at the compressed layer formed during the collision is higher than in the nonevolved case, and this could be important for triggering star formation processes. Furthermore, the wakes developed during the cloud evolution limit the reexpansion, so that after the collision in case 2 the merged clouds end up forming a smaller and denser region. In cases where self-gravity is dynamically important, the wake effect could play a fundamental role, reducing the expansion velocity of the material below the escape threshold and thus making it possible for the two clouds to build up a new, larger, gravitationally bound structure (see also Dinge 1997 for similar behavior in a single, moving, self-gravitating cloud).

The outcome of CCs is very different for the asymmetric cases, i.e., differently evolved clouds, even though our collisions all involve clouds of equal mass and head-on collisions. In this case, we obtain fragmentation of the "younger" cloud and the formation of a small expanding cloudlet that eventually dissolves into the WIM. As shown in Figure 9, in this case only part of the initial kinetic energy is radiated away during the collision. As a result, the remainder of the merged cloud material reexpands and, through interaction with the wake flow, becomes concentrated into dense clumps. At the end, most of the cloud material has been converted into the WIM, its directed kinetic energy being lost partly to radiation and partly to turbulent gas motion. KMW have shown that by slightly perturbing the surface of one of the two colliding clouds, the bending mode instability causes fragmentation rather than coalescence. In our study, the asymmetry in the problem is due to a slight difference in the evolutionary ages of the clouds ($0.5\tau_{cr}$). As already pointed out, its effect is comparable to that of an off-center collision. That is, the mass and momentum of the two clouds at impact have significantly different Y-distributions. Those structural differences of the clouds make the outcome of the collision very different from the symmetric cases. From this fact, we conclude that supersonic radiative collisions of clouds with the same gross characteristics (mass, speed, and structure), but without high symmetry, are disruptive and generate irregular filamentary clumps. On the other hand, previous results show

that collisions of clouds with major structure differences (density, size) are likely to be disruptive as well (Hausman 1981; Gilden 1984; Kimura & Tosa 1996; RFM). Our results support this. In addition, our results show that the adiabatic case, which applies to small clouds, will be highly disruptive, even if the clouds are identical and the collision head-on. Also, as pointed out below, off-center collisions, which are the most common, are certainly very unlikely to produce coalescence of clouds, at least for non–self-gravitating objects.

These results have an important impact on the ISM of galaxies. In general, supersonic, gasdynamical CCs tend to be disruptive, so that any model that tries to explain cloud evolution and the mass spectrum has to take these findings into account. If colliding clouds are sufficiently electrically conductive, then the presence of a large-scale magnetic field may play an important dynamical role in the interaction. It is not obvious, however, that our main conclusion will be altered. We have fully MHD simulations underway that will address that point in a separate report.

It is worthwhile to mention that our asymmetric calculations can provide some insights into off-center collisions as well, at least for those with a small impact parameter ($b \ll R_c$). In fact, with regard to the survival of the clouds, the most important implication for small impact parameter off-center collisions is probably asymmetry. For these cases, the results of our asymmetric calculations may apply as a guide, at least for clouds of comparable mass. However, when the impact parameter $b \sim R_c$, only part of the cloud is involved in the collision, and our calculations are not appropriate anymore. LMPS have investigated off-center, isothermal collisions for very massive clouds, including gravity in their calculations. They show that, for high relative velocity, the colliding parts of the clouds soon reexpand and disperse after the compression phase, whereas the outer parts (which do not get involved in the collision) proceed unhindered and form two new small clouds. On the other hand, for low relative velocity, the colliding clouds coalesce, whereas the outer gas motion is deflected into a circular pattern. As a result, rotating bound systems and bars form. For smaller non–self-gravitating clouds, we think that, in addition to the relative velocity, the adiabaticity is a key parameter. If $b \leq R_c$, the collision can probably be classified in terms similar to a highly asymmetric one. On the other hand, if $b \geq R_c$, the LMPS calculations suggested that the outer part of the clouds are torn apart during the collision. For an adiabatic collision, pressure waves in the remaining clouds generated during the encounter might be able to make the clouds expand and disperse into the WIM. However, in a strongly radiative encounter these waves could be damped away by radiation and the cloud cores might survive, although the clouds themselves would turn out quite distorted. Finally, if $b \sim 2R_c$, the collision will produce only minor perturbations on the cloud structures.

Of course, real clouds are three dimensional. CC three-dimensional calculations have been performed by Hausman (1981), LMPS, and Lattanzio & Henriksen (1988, hereafter LH); these authors, using a smoothed particle hydrodynamics code, investigate on the effects of several parameters (relative velocity, cloud mass ratio, impact parameter, and so on) on coalescence. Hausman's calculations are affected strongly by the limitations of his computational means. In particular, he used a resolution as low as 100 particles per cloud, and his calculations show unphysical particle interpenetration. For this reason, for example, in his run 1, Hausman finds a ratio $\rho_{\max}/\rho_{\rm ext}$ of only 3.55, much less than 50 as found by LMPS for the same case. As a result, little conversion of kinetic energy into thermal energy takes place; it is probably for this reason that, in most of his runs, Hausman finds that the cooling is efficient enough to ensure isothermality (Hausman 1981). Since the set of cases studied by Hausman is very similar to that presented by LMPS, we will neglect to go into more details about his results. LMPS employed a better version of the smoothed particle hydrodynamics code (Monaghan & Lattanzio 1985) and higher resolution ($\sim$2000 particles per cloud). We have already summarized their results regarding off-center collisions. They also found that symmetric head-on collisions generate a single rapidly reexpanding or collapsing cloud depending on whether the initial clouds are gravitationally stable or unstable, respectively. In asymmetric (but still head-on) cases, however, they concluded that even when a cloud is marginally stable to gravitational collapse, the collision with a smaller cloud (ratio of masses larger than 2.5; their clouds had the same density) does not initiate the instability. Finally, LH further investigated this problem by showing how spin and orbital angular momenta are important in determining the outcome of CCs. The accuracy of these results, although useful and to some extent in agreement with previously cited works and our own, is still limited by low resolution ($\sim$2000–3000 particles) and by some assumptions that are not always appropriate. Some of these were mentioned by the authors themselves. In addition, based on Hausman's (1981) results, both LMPS and LH assumed isothermal clouds, using $\gamma = 1$; but as already pointed out, this approach is not correct because of the fundamental dynamical role played in the reexpansion phase by thermal energy stored during the compression phase. That aspect is apparent in our results. In our radiative head-on symmetric simulations, which allow for a release of energy through radiative processes, the collisions produce a new merged stable cloud instead of a rapidly reexpanding cloud as found by LMPS. Also LMPS and LH do not include in their calculations an intercloud medium. However, as we have noted, the interaction of cloud material with the intercloud gas, particularly with shocks and cloud wakes, affects the evolution of the collision significantly.

Useful insights about how an additional degree of freedom in this problem might modify two-dimensional results may be provided by three-dimensional studies of some related problems. For example, Xu & Stone (1995) examined the evolution in three dimensions of a gas cloud overrun by a plane shock. They found behaviors qualitatively consistent with two-dimensional simulations of that problem (e.g., Bedogni & Woodward 1990; Jones & Kang 1993; KMW). In many respects, a shocked cloud is similar to a supersonic cloud in its evolution (Jones et al. 1994). Lee et al. (1996) have carried out a three-dimensional study of two colliding gas streams that is similar in some ways to collisions between clouds. They found, as we do for adiabatic collisions, that the bulk of the kinetic energy is converted into thermal pressure, and that this causes the colliding material to expand as it drives a shock into the ambient medium. Generally, the extra dimension will allow more complex motions to develop, and some considerations will depend quantitatively on the third dimension, but we see no evidence in the existing literature that the general

conclusions of the present work will be invalidated when it is included.

6. CONCLUSIONS AND SUMMARY

To summarize, in this paper we have found the following results for the gasdynamical collisions between two mildly supersonic interstellar clouds, $M \geq 1.5$, of comparable mass:

1. Supersonic CCs are most often disruptive. In particular, adiabatic collisions, which involve small clouds ($R_c <$ 0.4 pc, for the standard WIM parameters assumed in our calculations), always turn out to be disruptive.

2. For completely symmetric collisions, however, strong radiative energy losses can lead to coalescence of the two clouds. In fact, the emission of radiation reduces the thermal energy stored during the compression phase, preventing a vigorous pressure-driven reexpansion.

3. Asymmetry in the clouds at impact greatly enhances the tendency for clouds to be disrupted during the interaction, even when radiative cooling is strong. This is true even for a very modest asymmetry. In the adiabatic, asymmetric case, the clouds are almost immediately dispersed in the WIM. In the radiative case, new filamentary structures are produced out of the initial cloud material.

4. Future numerical work should not neglect the importance of allowing the clouds to develop a self-consistent structure, especially bow shocks and wakes, since these features strongly influence the interaction and add important hydrodynamical features. In particular, bow shock interaction of the colliding clouds produces higher compression, particularly in the adiabatic case. On the other hand, the wakes behind the clouds reduce the reexpansion along the X-axis, increasing the probability for coalescence.

F. M. devotes his efforts in this work to the memory of his friend Leonardo Muzzi, a young artist of deep perspective, who inspired his way of studying science. The work by T. W. J. and F. M. was supported in part by the NSF through grants AST 93-18959 and INT-9511654, and by the University of Minnesota Supercomputer Institute. The work by D. R. was supported in part by the Seoam Scholarship Foundation. A. F. acknowledges the hospitality of the University of Minnesota where this work started.

REFERENCES

Bedogni, R., & Woodward, P. 1990, A&A, 231, 481
Cowie, L. L. 1980, ApJ, 236, 868
Dickey, J. M., & Garwood, R. W. 1989, ApJ, 341, 201
Dinge, D. 1997, ApJ, 479, 792
Dohm-Palmer, R. C., & Jones, T. W. 1996, ApJ, 471, 279
Doroshkevich, A. G., & Zeldovich, Ya. B. 1981, Soviet Phys.—JETP Lett., 53, 405
Ferrara, A. 1993, ApJ, 407, 157
Ferrara, A., & Field, G. B. 1994, ApJ, 423, 665
Field, G. B., & Hutchings, J. 1968, ApJ, 153, 737
Field, G. B., & Saslaw, W. C. 1965, ApJ, 142, 568
Fleck, R. C. 1996, ApJ, 458, 739
Frank, A., Jones, T. W., Ryu, D., & Gaalaas, J. B. 1996, ApJ, 460, 777
Gilden, D. L. 1984, ApJ, 279, 335
Harten, A. 1983, J. Comput. Phys., 49, 357
Hausman, M. A. 1981, ApJ, 245, 72
———. 1982, ApJ, 261, 532
Hunter, J. H., Sandford, M. T., II, Whitaker, R. W., & Klein, R. I. 1986, ApJ, 305, 309
Jones, T. W., & Kang, H. 1993, ApJ, 402, 560
Jones, T. W., Kang, H., & Tregillis, I. L. 1994, ApJ, 432, 194
Jones, T. W., Ryu, D., & Tregillis, I. L. 1996, ApJ, 473, 365
Kimura, T., & Tosa, M. 1996, A&A, 308, 979
Klein, R. I., McKee, C. F., & Woods, D. T. 1995, in ASP Conf. Ser. 80, The Physics of Interstellar Medium and Intergalactic Medium, ed. A. Ferrara, C. Heiles, C. McKee, & P. Shapiro (San Francisco: ASP), 366 (KMW)
Lattanzio, J. C., & Henriksen, R. N. 1988, MNRAS, 232, 565 (LH)
Lattanzio, J. C., Monaghan, J. J., Pongracic, H., & Schwarz, M. P. 1985, MNRAS, 215, 125 (LMPS)
Lee, H., Kang, H., & Ryu, D. 1996, ApJ, 464, 131
LeVeque, R. J. 1997, in 27th Saas-Feé Advanced Course Lecture Notes, Computational Methods in Astrophysical Fluid Flows (Berlin: Springer), in press
McKee, C. F. 1990, in ASP Conf. Ser. 12, The Evolution of the Interstellar Medium, ed. L. Blitz (San Francisco: ASP), 3
Monaghan, J. J., & Lattanzio, J. C. 1985, A&A, 149, 135
Mousumi, D., & Chanda, J. J. 1996, ApJ, 462, 309
Norman, C. A., & Ferrara, A. 1996, ApJ, 467, 280
Oort, J. H. 1954, Bull. Astron. Inst. Netherlands, 12, 177
Penston, M. V., Munday, V. A., Stickland, D. J., & Penston, M. J. 1969, MNRAS, 142, 355
Pumphrey, W. A., & Scalo, J. M. 1983, ApJ, 269, 531
Ricotti, M., Ferrara, A., & Miniati, F. 1997, ApJ, 485, 254 (RFM)
Ryu, D., Ostriker, J. P., Kang, H., & Cen, R. 1993, ApJ, 414, 1
Schiano, A. V. R., Christiansen, W. A., & Knerr, J. M. 1995, ApJ, 439, 237
Smith, J. 1980, ApJ, 238, 842
Solomon, P. M., & Rivolo, A. R. 1989, ApJ, 339, 919
Spitzer, L. 1978, Physical Processes in the Interstellar Medium (New York: Wiley)
Stone, M. E. 1970a, ApJ, 159, 277
———. 1970b, ApJ, 159, 293
Strang, G. 1968, SIAM J. Numer. Anal., 5, 506
Struck-Marcell, C., & Scalo, J. M. 1984, ApJ, 277, 132
van Leer, B. 1976, J. Comput. Phys., 23, 276
Vazquez-Semadeni, E., Passot, T., & Pouquet, A. 1995, ApJ, 441, 702
Vietri, M., Ferrara, A., & Miniati, F. 1997, ApJ, 483, 262
Vishniac, E. T. 1994, ApJ, 428, 186
Xu, J., & Stone, J. M. 1995, ApJ, 454, 172